Supplement of Solid Earth, 6, 1045–1061, 2015
http://www.solid-earth.net/6/1045/2015/
doi:10.5194/se-6-1045-2015-supplement

Solid Earth
Open Access

Supplement of

Pinch and swell structures: evidence for strain localisation by brittle–viscous behaviour in the middle crust

R. L. Gardner et al.

Correspondence to: R. L. Gardner (robyn.gardner@mq.edu.au)

St. Anne Point Petrology

Swell centre samples e.g. AS1331I (see Fig. 1d): Mineral modal percentages of the swell centre comprise amphibole (69 area %), biotite (16 area %), quartz and plagioclase (7 area %) and accessory chlorite, calcite and opaques (together 8 area %). Amphibole and biotite (to 1.2 mm) define the foliation. Euhedral to anhedral, up to 2.5 mm, amphibole grains exhibit rare fracturing and some twinning. Fractures are narrow and filled with quartz and lesser calcite. Quartz grains are anhedral to 1 mm and commonly fill areas between amphibole grains with small dihedral angles (20^{o}). Quartz grains display minor undulose extinction and irregular boundaries.

Neck samples e.g. AS1331G (see Fig. 1e): Mineral modal percentages of the neck samples comprise amphibole and garnet (55 area %), biotite (26 area %), quartz and plagioclase (16 area %) and accessory epidote and opaques (together < 3 area %). Narrow, (< 0.10 mm) intensely sheared regions (Fig. 1e yellow lines) at 30 to 40^{o} from the primary stress direction occur in sets. Anhedral amphibole grains, up to 2 mm, define the foliation, with larger, up to 4 mm grains having been fractured (Fig. 1e asterisks) in intensely sheared regions. Fractured amphibole grains are more common than in the swell centre samples. Early quartz (Fig. 1e Qz_A) grains are anhedral to 1 mm with small dihedral angles (20^{o}) while early biotite (Fig. 1e Bt_A) is foliation parallel to 0.6 mm. These both commonly fill areas between amphibole grains. Later fine-grained quartz (Qz_B) to 0.05 mm and elongate biotite (Bt_B) to 0.20 mm have formed in the narrow, (< 0.10 mm) intensely sheared regions (Fig. 1e). Poikiloblastic garnet grains are up to 3.2 mm wide. Quartz grains display undulose extinction, subgrains and commonly have irregular boundaries.

Country rock samples e.g. AS1409A (see Supplementary Figure 1): Mineral modal percentages of the country rock samples comprise garnet (18 area %), biotite (30 area %), quartz (48 area %) and accessory plagioclase and opaques (together ~ 4 area %). Garnet grains occur in bands parallel to foliation and commonly display brittle fracturing at angles up to 30° from the foliation. Quartz grains are anhedral to 0.50 mm with strong shape preferred orientation and form foliation parallel ribbons. In association with garnet grains, the quartz grains display less shape preferred orientation. Biotite is elongate to 0.35 mm and generally parallel to foliation. Where it occurs in the garnet layer, biotite is parallel to the garnet fracture zones and is found in strain shadows. Biotite and quartz outside the garnet layers commonly form an S-C fabric. Overall foliation is defined by biotite and quartz ribbons with foliation parallel layers of garnet. Quartz grains display undulose extinction, subgrains and commonly have irregular boundaries.

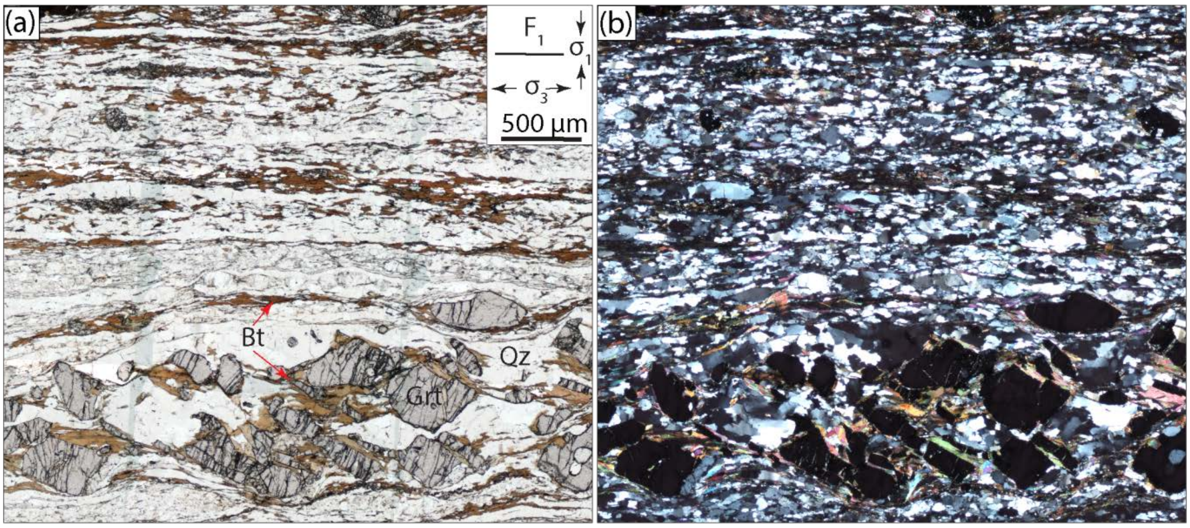

Figure S1: St Anne Point country rock of quartz, biotite and plagioclase showing S-C fabric and garnet grains with brittle fractures and strain caps/shadows. In quartz and feldspar grains, undulose extinction, subgrains and irregular, curved boundaries suggest dynamic recrystallization involving crystal plasticity, subgrain formation and grain boundary migration pointing to non-Newtonian flow in the country rock.

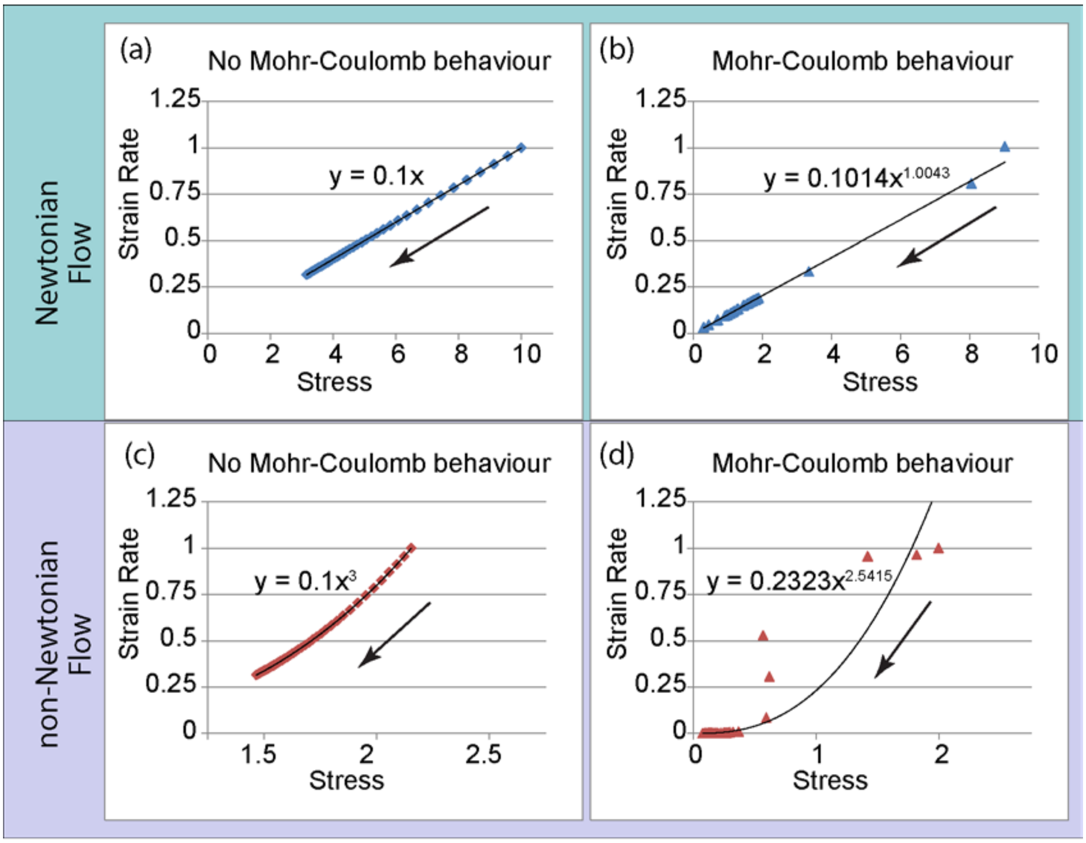

Figure S2: Graphs of Newtonian (a, b) and non-Newtonian (c, d) flow with Mohr-Coulomb strain localising behaviour (b and d) and with no Mohr-Coulomb behaviour (a, c). Relationship equations on (a) and (c) indicate the numerical system used is working as expected for Newtonian and non-Newtonian flow regimes. Black arrows indicate increasing simulation step numbers, i.e. increasing stretch.

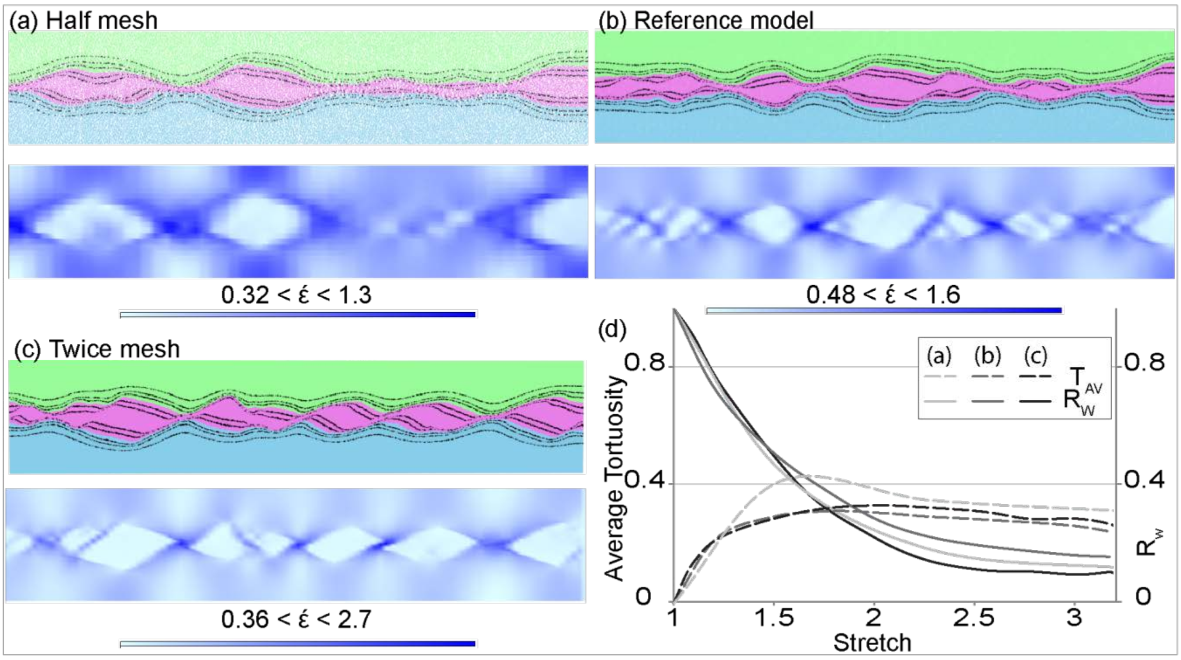

Figure S3: Testing the influence of mesh size on results. The model used for Figure 5a, which uses $R_v = 20$ and Newtonian flow, has been run at half (a) and double (c) the mesh size of the reference model (b). Layer and strain rate plots have been included at stretch 2.3 from each model. Development of maximum swell width to minimum neck width (R_W, equation 6) and average tortuosity versus stretch of the central layer edge are included in (d). Graphs show the tortuosity and R_W measurements used in this manuscript appear to be largely mesh independent while the numbers and spacing of swells, measurements not used in this paper, are mesh dependent.

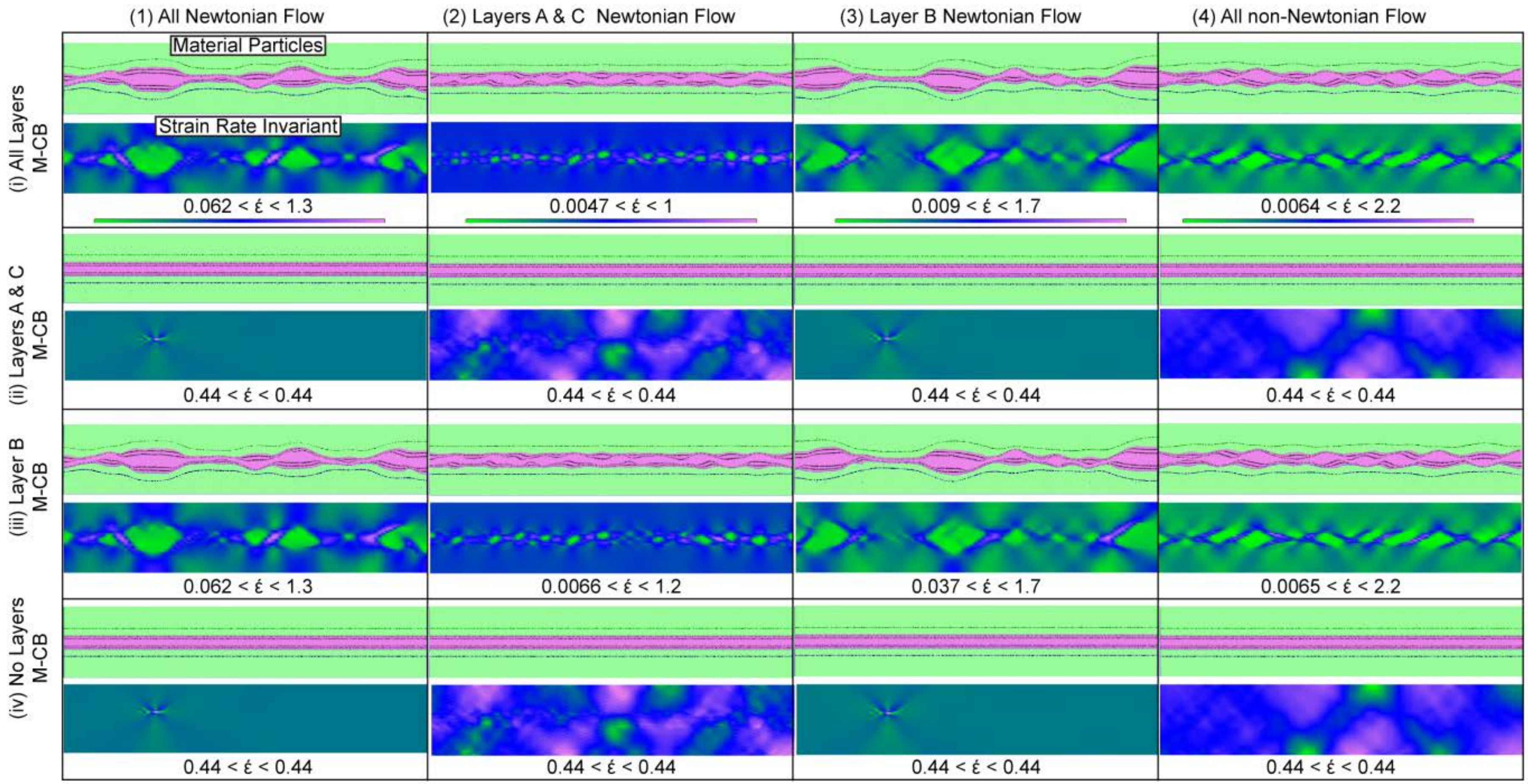

(1) All Newtonian Flow
(2) Layers A & C Newtonian Flow
(3) Layer B Newtonian Flow
(4) All non-Newtonian Flow
(i) All Layers M-CB
(ii) Layers A & C M-CB
(iii) Layer B M-CB
(iv) No Layers M-CB
Material Particles
Strain Rate Invariant
0.062 < ε̇ < 1.3
0.0047 < ε̇ < 1
0.009 < ε̇ < 1.7
0.0064 < ε̇ < 2.2
0.44 < ε̇ < 0.44
0.44 < ε̇ < 0.44
0.44 < ε̇ < 0.44
0.44 < ε̇ < 0.44
0.062 < ε̇ < 1.3
0.0066 < ε̇ < 1.2
0.037 < ε̇ < 1.7
0.0065 < ε̇ < 2.2
0.44 < ε̇ < 0.44
0.44 < ε̇ < 0.44
0.44 < ε̇ < 0.44
0.44 < ε̇ < 0.44

Figure S4: Analysis II result representations: Numerical results at stretch 2.3 where Newtonian/non-Newtonian flow and Mohr-Coulomb behaviour (M-CB) characteristics of layer B have been varied systematically with respect to layers A & C (for summary see Table 2). All models have $R_V = 10$. Strain rate invariant ($\dot{\varepsilon}$) ranges of values are as specified while range of colour is the same for all results: colour bars are included at (i) all layers M-CB.

Supplementary Table:

Material	Stress Exponent (n)
Quartz aggregate[1]	3.9 ± 0.8 to 4.1 ± 0.7
Feldspar aggregate[2]	3.0 ± 0.1
Olivine[3]	3.0 ± 0.1
Pyroxene aggregate[4]	4.7 ± 0.2
Natural marble[5]	1.7 ± 0.5 to 3.5 ± 0.6

Supplementary Table 1

Table S1. Experimentally determined stress exponents (n) for various materials undergoing non-Newtonian flow. References are: 1. Gleason and Tullis (1995); 2. Rybacki and Dresen (2004); 3. Mei and Kohlstedt (2000); 4. Bystricky and Mackwell (2001); 5. Rybacki et al. (2003).

References

Bystricky, M., and Mackwell, S.: Creep of dry clinopyroxene aggregates, Journal of Geophysical Research: Solid Earth, 106, 13443-13454, 10.1029/2001jb000333, 2001.

Gleason, G. C., and Tullis, J.: A flow law for dislocation creep of quartz aggregates determined with the molten salt cell, Tectonophysics, 247, 1-23, http://dx.doi.org/10.1016/0040-1951(95)00011-B, 1995.

Mei, S., and Kohlstedt, D. L.: Influence of water on plastic deformation of olivine aggregates: 1. Diffusion creep regime, Journal of Geophysical Research: Solid Earth, 105, 21457-21469, 10.1029/2000jb900179, 2000.

Rybacki, E., Paterson, M. S., Wirth, R., and Dresen, G.: Rheology of calcite–quartz aggregates deformed to large strain in torsion, Journal of Geophysical Research: Solid Earth, 108, 2089, 10.1029/2002jb001833, 2003.

Rybacki, E., and Dresen, G.: Deformation mechanism maps for feldspar rocks, Tectonophysics, 382, 173-187, 2004.